

## Effect of surface site on the spin state for the interaction of NO with Pd<sub>2</sub>, Rh<sub>2</sub> and PdRh nanoparticles supported at regular and defective MgO (001) surfaces

S.Abdel Aal\*<sup>1,2</sup>

<sup>1</sup>Department of Chemistry, Faculty of Science and Arts, Qassim University,  
P.O.Box 6666, Qassim, Buraidah, (SAUDIA ARABIA)

<sup>2</sup>Department of Chemistry, Faculty of Science, Benha University, P.O.Box 13518, Benha, (EGYPT)  
E-mail: safabdelaal@yahoo.com

**Abstract** : An attempt has been made to analyze the effect of surface site on the spin state for the interaction of NO with Pd<sub>2</sub>, Rh<sub>2</sub> and PdRh nanoparticles that supported at regular and defective MgO (001) surfaces. The adsorption properties of NO on homonuclear, Pd<sub>2</sub>, Rh<sub>2</sub>, and heteronuclear transition metal dimers, PdRh, that deposited on MgO (001) surface have been studied by means of hybrid density functional theory calculations and embedded cluster model. The most stable NO chemisorption geometry is in a bridge position on Pd<sub>2</sub> and a top configuration of Rh<sub>2</sub> and PdRh with N-down oriented. NO prefers binding to Rh site when both Rh and Pd atoms co-exist in the PdRh. The natural bond orbital analysis (NBO) reveals that the electronic structure of the adsorbed metal represents a qualitative change with respect to that of the free metal. The adsorption properties of NO have been analyzed with reference to the NBO, charge transfer, band gaps, pairwise and non-pairwise additivity.

The binding of NO precursor is dominated by the  $E_{(i)}^{M_x-NO}$  pairwise additive components and the role of the support was not restricted to supporting the metal. The adsorbed dimers on the MgO surface lose most of the metal-metal interaction due to the relatively strong bond with the substrate.

Spin polarized calculations were performed and the results concern the systems in their more stable spin states. Spin quenching occurs for Rh atom, Pd<sub>2</sub>, Rh<sub>2</sub> and PdRh complexes at the terrace and defective surfaces. The adsorption energies of the low spin states of spin quenched complexes are always greater than those of the high spin states. The metal-support and dimer-support interactions stabilize the low spin states of the adsorbed metals with respect to the isolated metals and dimers. Although the interaction of Pd, Rh, Pd<sub>2</sub>, Rh<sub>2</sub> and PdRh particles with Fs sites is much stronger than the regular sites O<sup>2-</sup>, the adsorption of NO is stronger when the particular dimers are supported on an anionic site than on an Fs site of the MgO (001). The encountered variations in magnetic properties of the adsorbed species at MgO (001) surface are correlated with the energy gaps of the frontier orbitals. The results show that the spin state of adsorbed metal atoms on oxide supports and the role of precursor molecules on the magnetic and binding properties of complexes need to be explicitly taken into account.

© Global Scientific Inc.

**Keywords** : Surface reactions; NO; Bimetallic nanoparticles; Spin state; Charge transfer.

# ORIGINAL ARTICLE

## INTRODUCTION

Fundamental understanding of the electronic structure and activity of transition metal atoms and nanoclusters supported on metal-oxide surfaces is of great interest due to their broad applications in catalysis, coating for thermal applications, corrosion protection, and other technologically important fields<sup>[1-4]</sup>. Theoretical calculations have proved very helpful to gain insight into the mechanisms of growth of nanoclusters on oxide surfaces<sup>[5,6]</sup>. It has been found that under typical conditions, formation of dimers constitutes the first step in the process of the growth of metal clusters on the oxide surface<sup>[7]</sup>. Even though in the gas phase there are dimers, trimers, etc., the cluster growth on the surface of the support is dominated by diffusion of adsorbed atoms and not by direct deposition of already existing gas phase clusters. It is observed that, diffusion is stopped at point defects, where the atoms are more strongly bound and nucleation takes place<sup>[8]</sup>. In addition, the properties of the deposited nanoclusters depend on the oxide substrate and in particular on the presence of point defects where the cluster can be stabilized. In general, there has been a consensus that defects not only can act as catalytic centers for chemisorption of small species but also as nucleation centers for growing metal clusters and can modify the catalytic activity of these adsorbed metal particles via the metal-support interaction at the interface<sup>[9]</sup>.

The strength of interaction between metal and substrate is due to metal-substrate covalent bonding that implies a polarization of the metal orbitals or redistribution of the atomic orbital population. The metal s-orbital combines with the oxygen p-orbital perpendicular to the surface of an oxide material resulting in a bonding (occupied) and antibonding (unoccupied) combinations. This leads to a decrease in the atomic s population of the metal atom<sup>[9-11]</sup>. When the free metal atom electronic configuration is  $d^n s^2$ , the resulting electronic configuration of the metal and atom may be expressed as  $d^{n+1} s^1$  or even  $d^{n+2}$ . The strength of the metal-oxide interaction varies with the resulting d-population. This change in the electronic configuration of the adsorbed metal may result in a concomitant spin quenching with respect to the ground state multiplicity of the isolated metal atom.

On the basis of the performance of different density functionals, Markovits et al.<sup>[12]</sup> reported that the electronic state of Ni with the oxygen regular and defective sites of MgO is the result of a balance between the tendency of Hund's rule to preserve the atomic state and chemical covalent terms tending to form chemical bonds and hence to quench the atomic magnetic moment. Indeed, the stronger the interaction, the smaller the difference between the high and low spin states; in other words, the larger the interaction, the stronger the spin quenching.

Sousa et al.<sup>[13]</sup> calculated the low to high spin transition energy of Ni adsorbed on regular and defective sites of MgO and magnetic properties of first row transition metal oxides. The previous investigations suggest that the final spin state of an adsorbed metal can be different, when it interacts with an oxide support. However, the combined effect of oxide support and adsorbed species, such as NO on the final spin state is overlooked.

Bimetallic nanoparticles may create a synergistic catalytic effect that involves the change in local electronic properties of pure metal nanoparticles to modify the strength of the surface adsorption for oxygen reduction reactions<sup>[14,15]</sup>. Although pure Pd and Rh clusters on MgO (001) and TiO<sub>2</sub> have been widely studied<sup>[16,17]</sup>, no reports are available on the geometrical and electronic structure of PdRh bimetallic that deposited on MgO surface. Efforts have been focused on the possibility of associating Pd with another noble metal, rhodium, to prepared bimetallic Pd-Rh/alumina catalysts and compared to reference Pd/alumina and Rh/alumina solids<sup>[18]</sup>. A. M. Ferrari<sup>[19]</sup>, Shinkarenko et al.<sup>[20]</sup>, Neyman and Illas<sup>[21]</sup>, Nasluzov et al.<sup>[22]</sup>, and Matveev et al.<sup>[23]</sup> have experimentally and theoretically studied the adsorption properties of different metal atoms and metal clusters deposited on the MgO (001) surface. Palladium and rhodium clusters of small size have been extensively studied at various semiempirical and ab initio levels of the theory by G. Berthier<sup>[24]</sup>. As the smallest cluster, homonuclear and heteronuclear transition metal dimers have been studied both experimentally and theoretically<sup>[25,26]</sup>. For a systematic theoretical study, the homonuclear dimers of 4d transition metals were examined by use of diverse density functional methods<sup>[27]</sup>. The structures of AgPd clusters supported

on MgO (001) are investigated via a combination of global optimization searches within an atom–atom potential model and density-functional calculations<sup>[28]</sup>. The reactions of H<sub>2</sub> with the heteronuclear dimers PdCu, PdAg, PdAu have been studied by the hybrid density functional method B3LYP<sup>[29]</sup>. CO adsorption on mono-metallic and bimetallic Au-Pd nanoparticles deposited onto well-ordered thin films of Fe<sub>3</sub>O<sub>4</sub> (111), MgO (001), and CeO<sub>2</sub> (111) were studied by<sup>[30]</sup>.

It is frequently observed that a transition metal atom doped in a small cluster of other metal can strongly change the properties of the host cluster<sup>[31,32]</sup>. Previous theoretical calculations have been devoted to the study of heteroatomic or impurity-doped as well as homoatomic metal clusters, which indicate that the impurity atoms can strongly influence geometric, electronic, and bonding properties of mixed clusters<sup>[33]</sup>. The first objective of this work is to generalize the possibility that electron-rich MgO surface can be used to determine how the substrate could affect the structural, energetic and electronic properties of small bimetallic Rh–Pd dimers that belonging to a completely different valence structure, i.e. Rh (4d<sup>8</sup> 5s<sup>1</sup>) with unfilled d and Pd (4d<sup>10</sup> 5s<sup>0</sup>) with complete d shell. For this purpose, the simplest bimetallic particle, PdRh, is considered and the results are compared with monometallic Pd<sub>2</sub> and Rh<sub>2</sub> dimers. Second, to clarify the roles of defects as nucleation centers for the formation of dimers and represent how these defects can induce modifications in the electronic, geometric and chemical properties of the supported dimers. Third, to identify the bonding mechanism of NO with Pd<sub>2</sub>, Rh<sub>2</sub> and PdRh nanoparticles that supported on regular and defective sites of MgO (001). Finally, to induce qualitatively different changes in the electronic states of the supported particles and on the transition energy required to switch from low spin to high spin state.

The intriguing heterogeneous processes associated with nitric oxide, NO, observed at transition metal and metal-oxide surfaces, are a continuous topic for research. The molecule, which is one of the simplest and most stable radicals, is spontaneously formed in combustion processes at elevated temperatures. Being a major environmental hazard, it is of vital importance to remove NO from the exhaust gases. The reduction of NO by CO on palladium is of practical interest and

experimental investigations show that nanosized palladium clusters have significant capacity to catalyze the CO + NO reaction at low temperatures<sup>[34,35]</sup>. As one of the key factors to understand the catalytic mechanism, the adsorption behaviors of NO on Pd clusters have been extensively studied<sup>[36,37]</sup>. Viñes et al. performed a combined experimental and theoretical study on the adsorption of NO on Pd nanoparticles, using infrared reflection adsorption spectroscopy (IRAS) and calculations based on density functional theory (DFT)<sup>[36]</sup>.

## COMPUTATIONAL DETAILS AND SURFACE MODELS

Hybrid density functional theory and embedded cluster models have been extensively employed in the description of the electronic and geometrical structures of Pd<sub>2</sub>, Rh<sub>2</sub> and PdRh particles nucleated on regular and defect sites on the MgO(001) surface<sup>[5,38,39]</sup>. These models have demonstrated to be powerful in the description of the defective and non defective non polar oxide surface<sup>[40]</sup>. Sousa, et al.<sup>[13]</sup> used a cluster/periodic comparison within the same computational model (either DFT or HF) for the ionic systems (MnO, FeO, CoO, NiO, and CuO) to establish that embedded cluster models provide an adequate representation. They used a lattice parameter (421 pm) the same as was determined for the bulk, with no surface relaxation or rumpling in the defect-free system. The embedded cluster model considers a finite cluster embedded in the rest of the host crystal, by assuming that the electronic structure in this external region has remained the same as in the defect free system. This approach is adequate in principle, but is computationally demanding and requires an accurate analysis of the energy terms. Its flexibility is moderate and can describe the charged defects<sup>[41]</sup>.

To represent the substrate, the ionic clusters Mg<sub>9</sub>O<sub>14</sub> and Mg<sub>9</sub>O<sub>13</sub>Fs have been embedded in arrays of point charges. This was done by following an embedding procedure previously reported for alkaline earth oxides<sup>[42]</sup>. A finite ionic crystal of 292 point charges was first constructed. The Coulomb potentials along the X and Y axes of this crystal are zero by symmetry as in the host crystal. The ± 2 charges on the outer shells were then modified, by using a fitting procedure;

# ORIGINAL ARTICLE

to make the Coulomb potential at the four central sites closely approximates the Madelung potential of the host crystal, and to make the Coulomb potential at the eight points with coordinates  $(0, \pm R, \pm R)$  and  $(\pm R, 0, \pm R)$  where  $R$  is half the lattice distance, which for MgO is 2.105, equal to zero as it should be in the host crystal. With these charges, 0.818566 and 1.601818, the Coulomb potential in the region occupied by the central ions is very close to that in the unit cell of the host crystal. The Coulomb potential was calculated to be (1.748) at the four central sites (compared with 1.746 for a simple cubic ionic crystal) and (0.0) at the previously defined eight points (compared with 0.0 for the same crystal). All charged centers with cartesian coordinates  $(\pm X)$ ,  $(\pm Y)$  and  $(Z > 0)$  were then eliminated to generate the (001) surface of MgO with 176 charged centers occupying the three dimensional space  $(\pm X)$ ,  $(\pm Y)$  and  $(Z > 0)$ . The clusters of Figure 2 were then embedded within the central region of the crystal surface, and the electrons of the embedded clusters were included in the Hamiltonians of the ab initio calculations. Other crystal sites entered the Hamiltonian either as full or partial point charges as demonstrated in<sup>[42]</sup>.

The density functional theory calculations were performed by using Becke's three parameter exchange functional B3 with LYP correlation functional<sup>[43,44]</sup>. The B3LYP hybrid functional has been used since it provides a rather accurate description of the metal/oxide interaction<sup>[45]</sup>. Moreover, for the magnetic systems it provides a reasonable albeit not perfect picture which lies midway between the HF and pure GGA descriptions<sup>[46]</sup>. Even if the DFT has well known problems with the description of magnetic properties, hybrid functionals such as B3LYP provides a fair indication of the relative energies. B3LYP correctly reproduce the thermochemistry of many compounds including transition metal atoms<sup>[47]</sup> and seems to be able to properly describe the band structure of insulators<sup>[12]</sup>. B3LYP ensures a correct description of the electronic ground state of first row transition metal atoms and a reasonable description of the energy difference between low lying electronic states with different spin multiplicity. Finally, B3LYP is able to describe magnetic coupling in systems with localized spins although the magnetic coupling constant is too large<sup>[48]</sup>.

The Stevens, Basch and Krauss Compact Effec-

tive Potential (CEP) basis sets<sup>[49,50]</sup> were employed in the calculations. In the CEP basis sets, the double zeta calculations are referred to as CEP-31G, and similarly triple zeta calculations to as CEP-121G. It may be noted that there is only one CEP basis set defined beyond the second row, and the two basis sets are equivalent for these atoms. These basis sets have been used to calculate the equilibrium structure and spectroscopic properties of several molecules and the results are compared favorably with the corresponding all-electron calculations<sup>[51]</sup>. In the present calculations, the effective core potential of the cep-121g basis set was used for all atoms in the clusters.

The defect free surfaces exhibit very small relaxations only and therefore they have been kept fixed when studying deposition of metal atoms. A minimal energy search on a defect free surface does not usually include surface relaxation since this is experimentally very small, less than 5%<sup>[52]</sup>. Surface relaxation effects can be significant if discontinuities, like steps or point defects, are present<sup>[53]</sup>. Sousa et al.<sup>[13]</sup> focused in the problems when applying DFT methods to open-shell systems with particular emphasis on the consequences on the description of magnetic properties. They found for ionic systems with unfilled d- shells, such as the present Rh atom, that the resulting open-shell electrons are localized and hence it is possible to model these systems by means of embedded cluster models. All calculations are of spin unrestricted type and carried out by using Gaussian 09 system<sup>[54]</sup>. The figures were generated by using the corresponding Gauss View software.

The binding energy,  $E_{a_2}$ , of the Pd<sub>2</sub>, Rh<sub>2</sub> and PdRh dimers at various sites of the metal oxide surface can be calculated as follows:

$$E_a(M_2) = -[E(M_2/MgO\_site) - E(M_2) - E(MgO\_site)] \quad (1)$$

Positive values of the binding energies mean that the formed dimers are stable.

The high to low spin transition energies were calculated from the relation

$$\Delta E_{\text{complex}}^{\text{H-L}} = E_{\text{complex}}^{\text{H}} - E_{\text{complex}}^{\text{L}} \quad (2)$$

Where  $E_{\text{complex}}$  is the total electronic energy of the complex.

The nucleation energy ( $E_{\text{nucl}}$ ), dimer formation energy, is an important parameter to study the atom-by-atom growth of a particle from atoms in the gas phase.

It is defined as the energy associated with the formation of homonuclear dimers  $\text{Rh}_2$ ,  $\text{Pd}_2$ , and heteronuclear dimers,  $\text{PdRh}$ , when an atom of the gaseous phase, Rh or Pd bonds with a pre-adsorbed metallic particle, Rh/MgO<sub>site</sub> or Pd/MgO<sub>site</sub><sup>[54]</sup>, respectively:

$$E_{\text{nucl}} = -[\text{E}(\text{M}_2/\text{MgO}_{\text{site}}) - \text{E}(\text{M}) - \text{E}(\text{M}/\text{MgO}_{\text{site}})] \quad (3)$$

where MgO<sub>site</sub> indicates the nucleation site. These two quantities,  $E_a(\text{M}_2)$  and  $E_{\text{nucl}}$ , measure the binding energy of gas phase  $\text{Pd}_2$ ,  $\text{Rh}_2$  and  $\text{PdRh}$  to a given MgO site<sup>[55]</sup>.

The dimer binding energy,  $E_b$ , measures the stability of the adsorbed dimer with respect to Pd and Rh adatoms, where one of which is bound on a five coordinated terrace anion,  $\text{O}_{5c}$ .  $E_b$  is simply the difference between the adsorption energy of transition metal, TM, atom to the supported TM/MgO and the binding energy of the atom to the metal oxide terrace.

$$E_b = -\text{E}(\text{M}_2/\text{MgO}_{\text{site}}) - \text{E}(\text{MgO}_{\text{O}_{5c}}) + \text{E}(\text{M}/\text{MgO}_{\text{site}}) + \text{E}(\text{M}/(\text{MgO}_{\text{O}_{5c}})) \quad (4)$$

The trapping energy,  $E_t$ , measures the energy gain when Pd and Rh atoms move from a terrace site to a strongly binding site, anion vacancy. The trapping energy is the difference in  $E_a$  between a regular and a defect site.  $E_t$  can be quite large on some specific defects, indicating their strong tendency to capture metal atoms. Thus, metal atoms have a high probability to find a defect in the diffusion process and to stick to this defect<sup>[56]</sup>.

## RESULTS AND DISCUSSION

### Adsorption of single Pd and Rh atoms

It was well established that small metal particles adsorb preferentially on sites where negative charge accumulates<sup>[6,39,57,58]</sup>; more specifically the  $\text{O}^{2-}$  ionic sites for regular and the  $\text{F}_s$  centers for defective metal oxide. Experimentally, metal clusters are often formed on a surface by exposing it to a beam of gas-phase atoms. These atoms adsorb onto the surface and diffuse to the sites at  $\text{O}^{2-}$  or  $\text{F}_s$  centers. From these single adsorbed atoms, clusters are formed by nucleation. For this reason, the adsorption of a single Pd and Rh atoms on both  $\text{O}^{2-}$  and  $\text{F}_s$  of MgO is investigated as a first step in this study. The results provide a clear indication that the atomic Rh adsorbs more strongly on both sites than

that of Pd. The interaction of Rh and Pd atom on F site is characterized by stronger binding energy ( $E_{\text{ads}} = 3.263$  eV, 3.186 eV) with shorter equilibrium adsorption distance (1.62 Å, 1.54 Å) than on the surface  $\text{O}^{2-}$  site ( $E_{\text{ads}} = 1.301$  eV, 1.251 eV) with equilibrium distance (2.06 Å, 2.19 Å), respectively. The presence of trapped electrons at the defect site results in a more efficient activation of the supported Pd and Rh atoms. These results are in agreement with<sup>[5,59,60]</sup>. In general, a good agreement is established between the geometrical parameters obtained in this work and the reported theoretical values for Rh/MgO (001) surface (2.09 Å<sup>[61]</sup>) and for Pd/MgO (001) (2.15 Å<sup>[62]</sup>) at the low coordinated surface.

In addition, it is not a trivial task to conclude a priori which one of the  $^4\text{F}$  ( $4d^8s^1$ ) and  $^2\text{D}$  ( $d^9$ ) states of Rh determines the ground state energy of the unit cell of MgO (001) surface with the adsorbed Rh atom. Therefore, the effect of the substrate on the electronic states of the adsorbate and the energy required to switch from high-spin to low-spin state are analyzed. By using the B3LYP calculation, high- to low-spin transition energies of Rh atoms free,  $\Delta E^{\text{H-L}}$ , and supported on  $\text{O}^{2-}$  and  $\text{F}_s$  sites of MgO (001),  $\Delta E_{\text{complex}}^{\text{H-L}}$ , are summarized in TABLE 1. Since  $\Delta E_{\text{complex}}^{\text{H-L}}$  is negative value, the spin-polarized structure with one unpaired electron is the most stable state, in agreement with<sup>[62]</sup>. Consequently, the interaction of Rh at MgO (001) surface induces a quenching of the magnetic moment, which results in a doublet ground state, separated by 0.267 eV from the lowest quartet. Whereas, upon interaction with  $\text{O}^{2-}$  and  $\text{F}_s$  surface sites, the high to low spin transition energies  $\Delta E_{\text{complex}}^{\text{H-L}}$  of Pd atom is positive indicating that the spin states are preserved and the low spin states are favored. Hence, the number of unpaired electrons in the Pd adatom tends to be the same as in the gas phase and the ground state of Pd–MgO is spin singlet. The interaction of Rh and Pd atoms with the  $\text{F}_s$  center merits a separate discussion since results show that in almost all cases  $\Delta E_{\text{complex}}^{\text{H-L}}$  exhibits the largest increase. Hence, it is clear that, the low-spin state is more favored because of the formation of a direct bond between the adsorbed species and the electronic levels corresponding to the oxygen vacancy electrons.

# ORIGINAL ARTICLE

**TABLE 1 :** Transition energy,  $\Delta E_{\text{complex}}^{\text{H-L}}$ , required to excite adsorbed monomer, Pd and Rh from the high- to low-spin state. A positive sign indicates that the ground state is provided by the low-spin coupling.  $\Delta d^{\text{H-L}}$  are the change in the equilibrium distances of Pd and Rh atoms that supported to the regular ( $\text{O}^{2-}$ ) and oxygen vacancy ( $\text{Fs}$ ) site at MgO (001) going from high- to low-spin state. A positive value indicates that d is larger in the high-spin state. Energies are expressed in eV, the corresponding equilibrium distances (d) in (Å), and charges in electron units H: High spin. L: Low spin. Ne: number of unpaired electrons.

	Pd/MgO ( $\text{O}^{2-}$ ) site	Pd/MgO (Fs) site	Rh/MgO ( $\text{O}^{2-}$ ) site	Rh/MgO (Fs) site
$\Delta E^{\text{H-L}}$		0.904		-0.034
$E_{\text{ads}}^{\text{H}}$ (M)	0.919	1.933	1.034	1.812
$d^{\text{H}}$ (M-S)	2.39	1.82	2.54	2.06
$\Delta E_{\text{complex}}^{\text{H-L}}$	1.234	2.156	0.232	1.417
$\Delta d^{\text{H-L}}$	0.2	0.28	0.48	0.44
Electronic configuration	$5s^{0.28}4d^{9.74}5p^{0.01}6p^{0.02}$	$5s^{0.79}4d^{9.86}5p^{0.14}5d^{0.01}6p^{0.02}$	$5s^{0.43}4d^{8.6}5p^{0.03}$ $5d^{0.01}6p^{0.01}$	$5s^{0.83}4d^{8.81}5p^{0.13}$ $5d^{0.02}6p^{0.02}$
Ne	10.05	10.82	9.05	9.81

Nevertheless, the important point here is the trend of the adsorbed atoms from one site to another. The analysis of these results clearly show that, there is a change in the transition energy required to switch from high spin to low spin,  $\Delta E_{\text{complex}}^{\text{H-L}}$ , which is induced by the MgO (001) surface. It is observed that the transition energy from the high-spin to the low-spin state increases when the oxide support is present. This is a clear indication that the metal-support interaction tends to stabilize the low-spin state with respect to the isolated atom. The difference in the equilibrium distance perpendicular to the surface was calculated. Notice that, as expected, there is an inverse correlation between adsorption energy and equilibrium distance, the larger the former the shorter the later, TABLE 1.

There are some differences in the adsorption heights between the lowest spin state and the highest spin state of the adsorbed Rh and Pd atoms on both the  $\text{O}_{\text{sc}}$  and oxygen vacancy sites. In particular, for the perfect surface, the adsorption height of 2.54 Å and 2.39 Å for the quartet Rh and triplet Pd that is larger by 0.48 Å and 0.2 Å than for the doublet Rh and singlet Pd, respectively. The similar phenomena for the vacancy surface are also observed. This observation may result from the larger overlaps between the highest occupied molecular orbital, HOMO, of MgO cluster and the lowest unoccupied molecular orbital, LUMO, of the adsorbed metal atoms in the doublet and singlet state than those in the quartet and triplet states of the adsorbed Rh and Pd atoms that have anti-bonding character as shown from Figure 1. Therefore, a short bond distance and a

strong interaction between the  $\text{O}^{2-}$  and Fs sites and the Rh and Pd atoms at the lowest spin state have been observed (TABLE 1).

The increase in the adsorption heights of supported Pd and Rh can contribute to the Pauli repulsion of the valence s orbital of the Pd and Rh that is almost empty with those in the p orbitals of the surface oxygen atoms. As well as, the HOMO for the oxygen vacancy has a large s-like character, which would also lead to repulsive interaction with the metal s orbital; this orbital is occupied by  $\sim -0.8$  e due to the charge transfer. The adsorption heights of supported Pd and Rh increased at oxygen anion and oxygen vacancy sites also the energy gain of 1.90 eV and 2.0 eV due to the electron occupying this bonding orbital of the Pd and Rh atom, where the binding energy is calculated to be 3.192 eV and 3.263 eV for the adsorption complexes Pd/Mg<sub>9</sub>O<sub>13</sub>Fs and Rh/Mg<sub>9</sub>O<sub>13</sub>Fs, respectively.

It is interesting to explore the electronic configuration for the interaction of Pd and Rh atoms with the regular site at MgO (001) surface. The only appreciable change with respect to the free atom is the hybridization between 5s and 4d orbitals with negligible contribution of the 5p subshell,  $5s^{0.28}4d^{9.74}5p^{0.01}6p^{0.02}$  and  $5s^{0.43}4d^{8.6}5p^{0.03}5d^{0.01}6p^{0.01}$  for the supported Pd and Rh atoms and no appreciable charge transfer, -0.054e and -0.07e, respectively, These results are consistent with<sup>[63]</sup>. The increased adsorption energy of Pd and Rh atoms with  $\text{F}_{\text{s}}$  centers is accompanied by notable changes in the electronic configuration of the adsorbed metal, which is progressively changed by a

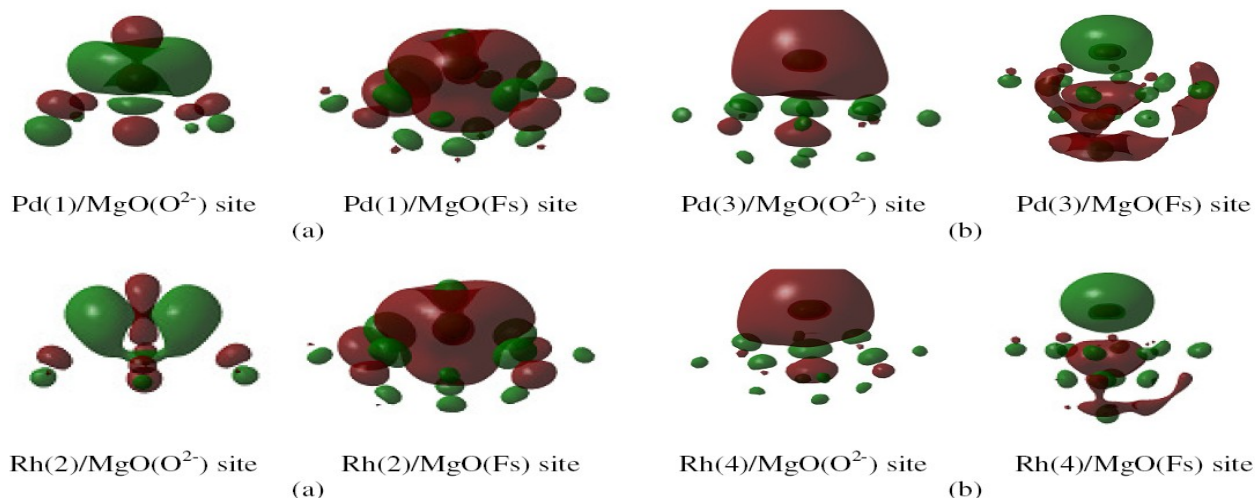


**Figure 1 :** Schematic representation of the highest occupied molecular orbitals (HOMOs) of Pd and Rh atoms with (a) low spin state and (b) high spin state deposited on  $\text{MgO}(\text{O}^{2-})$  and  $\text{MgO}(\text{Fs})$  sites using the embedded cluster model.

charge transfer,  $-0.799e$  and  $-0.807e$ , with an increasing participation of the  $5p$  orbitals, for the supported Pd and Rh atoms,  $5s^{0.79}4d^{9.86}5p^{0.14}$  and  $5s^{0.83}4d^{8.81}5p^{0.13}$ , respectively, TABLE 1.

As it has been shown later, the interaction of NO with supported Pd and Rh depends strongly on the metal–oxide interaction and it is essential to dispose of an adequate substrate model for the subsequent NO adsorption<sup>[64,65]</sup>. Hence, as a first step in our approach,  $\text{Rh}_2/\text{MgO}$  (001),  $\text{Pd}_2/\text{MgO}$  (001) and  $\text{PdRh}/\text{MgO}$  (001) systems were studied using the above detailed cluster models.

### **$\text{Rh}_2$ , $\text{Pd}_2$ and $\text{PdRh}$ particles deposited on $\text{MgO}$ (001)**

To underscore the most stable configuration of  $\text{Rh}_2$ ,  $\text{Pd}_2$  and  $\text{Pd-Rh}$  dimer on the  $\text{MgO}$  (001) surface, two configurations, parallel and perpendicular to the surface plane have been considered. The best optimized geometries of  $\text{Rh}_2$ ,  $\text{Pd}_2$  and  $\text{PdRh}$  supported particles anchored on terrace sites of  $\text{MgO}$  (001) are with the molecular axis almost parallel to the surface and the supported two atoms of the dimer nearly on the top of two  $\text{O}_{5c}$  anions, Figure 2. The results are agreement with<sup>[19,56,66]</sup>.

Because of the spin polarization, the corresponding values of binding, nucleation, trapping and charges transfer for the deposition of the  $\text{Rh}_2$ ,  $\text{Pd}_2$  and  $\text{PdRh}$  particles on the regular oxygen site and Fs center have been summarized in TABLE 2 by using B3LYP/CEP-121G at various spin states in order to find the most

stable spin state for each dimer. It is interesting to note that, the ground state of  $\text{Rh}_2$ ,  $\text{Pd}_2$  is singlet, at variance with gas-phase of  $\text{Pd}_2$  and  $\text{Rh}_2$  which has a triplet  $^3\Sigma_u^{+}$ <sup>[67,68]</sup> and quintet  $^5\Sigma_u^{+}$ <sup>[69]</sup> ground state, respectively, but in agreement with previous studies<sup>[5,16]</sup>. Thus, the interaction with the substrate induces a change in the electronic structure of  $\text{Pd}_2$  and  $\text{Rh}_2$  dimers. The adsorption energies of  $\text{Rh}_2$ ,  $\text{Pd}_2$  and  $\text{PdRh}$  in the low spin states are stronger than those in the high spin states. Hence, the dimer–support interactions stabilize the low spin states of the adsorbed  $\text{Rh}_2$ ,  $\text{Pd}_2$  and  $\text{PdRh}$  dimers.

From these results, it is observed that the interaction of  $\text{Rh}_2$ ,  $\text{Pd}_2$  and  $\text{PdRh}$  on Fs site is characterized by stronger binding energy with shorter equilibrium adsorption distance than on the surface  $\text{O}^{2-}$  site. Although the binding energy is noticeably affected by the support, the nucleation energy is weakly affected; for both sites the values of  $E_{\text{nucl}}$  are less significantly changed (0.001 - 0.246 eV). This can mean that (a) the regular metal oxide surface is always an appropriated place to form  $\text{Rh}_2$ ,  $\text{Pd}_2$  and  $\text{Pd-Rh}$  (b) the dimers formation is independent of the adsorption site (regular or diamagnetic Fs site). However the dimer formation will be favored on the Fs center due to the trapping energy, consistently with<sup>[3]</sup>.

On a terrace site, the addition of second TM atom leads to a nucleation energy  $E_{\text{nucl}} = 1.716$  eV, 2.465 eV, and 2.354 eV that are 0.466 eV, 1.165 eV and 1.053 eV higher than the adsorption energies of the TM atom on a terrace site. Consequently, the dimer



## ORIGINAL ARTICLE

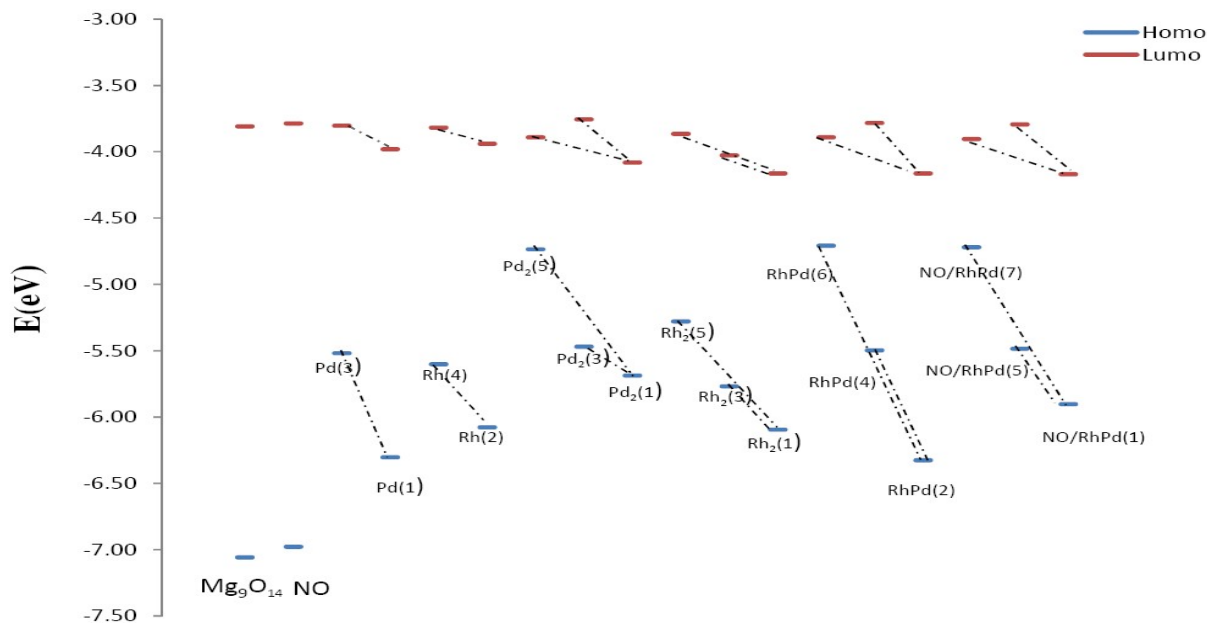


**Figure 2 :** Frontier orbitals of regular surfaces  $\text{Mg}_9\text{O}_{14}$ , free NO molecule, Pd/  $\text{Mg}_9\text{O}_{14}$ , Rh/  $\text{Mg}_9\text{O}_{14}$ ,  $\text{Pd}_2/\text{Mg}_9\text{O}_{14}$ ,  $\text{Rh}_2/\text{Mg}_9\text{O}_{14}$ , PdRh/  $\text{Mg}_9\text{O}_{14}$ , NO/Pd<sub>2</sub>/  $\text{Mg}_9\text{O}_{14}$ , NO/Rh<sub>2</sub>/  $\text{Mg}_9\text{O}_{14}$  and NO/PdRh/  $\text{Mg}_9\text{O}_{14}$  at their high and low spin states.

**TABLE 2 :** Geometrical parameters, binding, nucleation, trapping energies and atomic charges for the adsorption of Pd<sub>2</sub>, Rh<sub>2</sub> and PdRh dimers with various spin multiplicities at regular ( $\text{O}^{2-}$ ) site and defect center (Fs) site of the MgO (001) surface. Energies are expressed in eV, the corresponding equilibrium distances (d) in (Å), and charges in electron units.

	MgO ( $\text{O}^{2-}$ ) site									MgO (Fs) site								
	Pd <sub>2</sub>			Rh <sub>2</sub>			PdRh			Pd <sub>2</sub>			Rh <sub>2</sub>			PdRh		
	M=1	M=3	M=5	M=1	M=3	M=5	M=2	M=4	M=6	M=1	M=3	M=5	M=1	M=3	M=5	M=2	M=4	M=6
$E_a$ ( $M_2$ )	3.681	2.828	2.252	3.116	2.647	1.767	3.038	2.164	1.894	5.616	4.155	3.644	4.875	4.399	2.795	4.728	3.688	3.585
$E_{\text{nuc}}$	1.716	1.412	-0.894	2.465	2.653	2.502	2.354	2.139	4.647	1.717	0.804	-1.438	2.263	2.443	1.567	2.108	1.694	4.403
$E_b$	0.466	0.161	-2.145	1.165	1.352	1.201	1.053	1.071	2.119	0.466	-0.447	-2.688	0.962	1.142	0.267	0.807	0.659	-1.183
$E_{\text{trap}}$	-	-	-	-	-	-	-	-	-	2.489	1.328	1.392	3.116	2.647	1.767	3.038	2.164	1.894
$q(M_1)$	-0.069	0.03	-0.006	-0.064	-0.05	0.081	-0.01	0.008	-0.082	0.022	0.028	0.173	0.008	0.261	0.053	-0.001	-0.782	-0.842
$q(M_2)$	-0.029	0.069	0.233	-0.097	0.087	0.112	0.001	0.107	0.334	-0.78	-0.727	-0.674	-0.999	-1.005	-0.751	-0.803	0.09	0.312
$q(M_2)$	-0.098	0.099	0.227	-0.161	0.037	0.193	-0.009	0.115	0.252	-0.758	-0.699	-0.501	-0.991	-0.744	-0.698	-0.804	-0.692	-0.530
$d(M_1\text{-S})$	2.14	2.26	2.36	2.02	2.14	2.26	2.19	2.19	2.25	2.18	2.24	2.34	1.98	2.02	2.18	2.1	2.24	2.24
$d(M_2\text{-S})$	2.23	2.28	2.41	2.06	2.1	2.12	2.1	2.19	2.23	1.54	1.62	1.76	1.58	1.62	1.62	1.57	1.59	1.67

$q(M_1)$ ,  $q(M_2)$ : atomic charges at each metal of the dimer and  $d(M_1\text{-S})$ ,  $d(M_2\text{-S})$ : optimal distances between adsorbed metals of the dimer and surface site of MgO

formation of Rh<sub>2</sub>, Pd<sub>2</sub> and PdRh are preferred with respect to two isolated atoms adsorbed on  $\text{O}^{2-}$  anions (TABLE 2), indicating that dimerization should be possible even on the MgO (001) terraces and the dimer nucleation is a thermodynamic favored process at  $\text{O}^{2-}$  anions. Although this result is in contrast with the results reported by Bogicevic and Jennison<sup>[70]</sup> who reported almost no difference in stability between the dimer and two isolated atoms on the MgO (001) terraces, it is agreement with<sup>[5,66]</sup>.

The elongation of the Pd–Pd, Rh–Rh and Pd–Rh distances with respect to the gas-phase is explained by the fact that the dimer is oriented towards two nearest neighbor  $\text{O}^{2-}$  anions on the surface to maximize the bonding with the  $\text{O}^{2-}$  anions. The Pd–Pd bond length becomes close to 2.98 Å, is only 0.22 Å longer than in the free molecule, in agreement with<sup>[71]</sup>.

Concerning the bimetallic PdRh particle, the ground state geometry of the bimetallic is significantly modified after deposition. The electronic density of states analy-



sis reveals that after deposition, Pd–Rh favors doublet spin multiplicity as the lowest energy configuration, TABLE 2. In consequence, the binding, nucleation and dimer binding energies for Rh–Rh and Pd–Rh are very close. So that, such a comparison is of interest as many recent experimental studies on the supported palladium model catalytic systems<sup>[39]</sup> address the question whether the palladium can be used as an alternative to the expensive rhodium in the reaction of reduction of NO<sup>[72]</sup>.

In this section, the stability trends of the Pd<sub>2</sub>, Rh<sub>2</sub> and PdRh dimers for ground state structures are analyzed in terms of the energy gaps between HOMO and LUMO. A large HOMO–LUMO gap has been considered as an important requisite for the chemical stability of transition metal clusters<sup>[68]</sup>. The calculated HOMO–LUMO gaps for the ground states of Pd<sub>2</sub>, Rh<sub>2</sub> and PdRh dimers are presented in TABLE 2. It can be seen from this table that, the calculated HOMO–LUMO gaps of Pd<sub>2</sub>, Rh<sub>2</sub> and PdRh dimers follow the trend Pd<sub>2</sub> < Rh<sub>2</sub> < PdRh. Since a large energy gap corresponds

to higher stability therefore, the PdRh dimers that deposited on the MgO (O<sup>2-</sup>) and MgO (Fs) sites have the highest chemical stabilities.

Indeed, the molecular orbital, MO, interaction is controlled by the level of the frontier orbitals. Therefore, the relations between spin quenching of supported Rh, Pd, Pd<sub>2</sub>, Rh<sub>2</sub> and PdRh dimers at MgO surface and energy gaps between frontier orbitals are established. In Figure 3, the HOMOs and LUMOs of the supported metals and dimers at the defect free surface of MgO are presented. While spin preservation occurs for Pd complex, spin quenching occurs for Rh, Rh<sub>2</sub>, Pd<sub>2</sub> and RhPd complexes; this is agreement with TABLES 1-3. This is clearly correlated with frontier orbital energies where the HOMO energy levels of Rh, Rh<sub>2</sub>, Pd<sub>2</sub> and Pd–Rh low spin complexes are lower than their high spin counterparts. This extra stability allows for stronger interaction with the surface hence, the interaction in this case is strong enough to quench the spin.

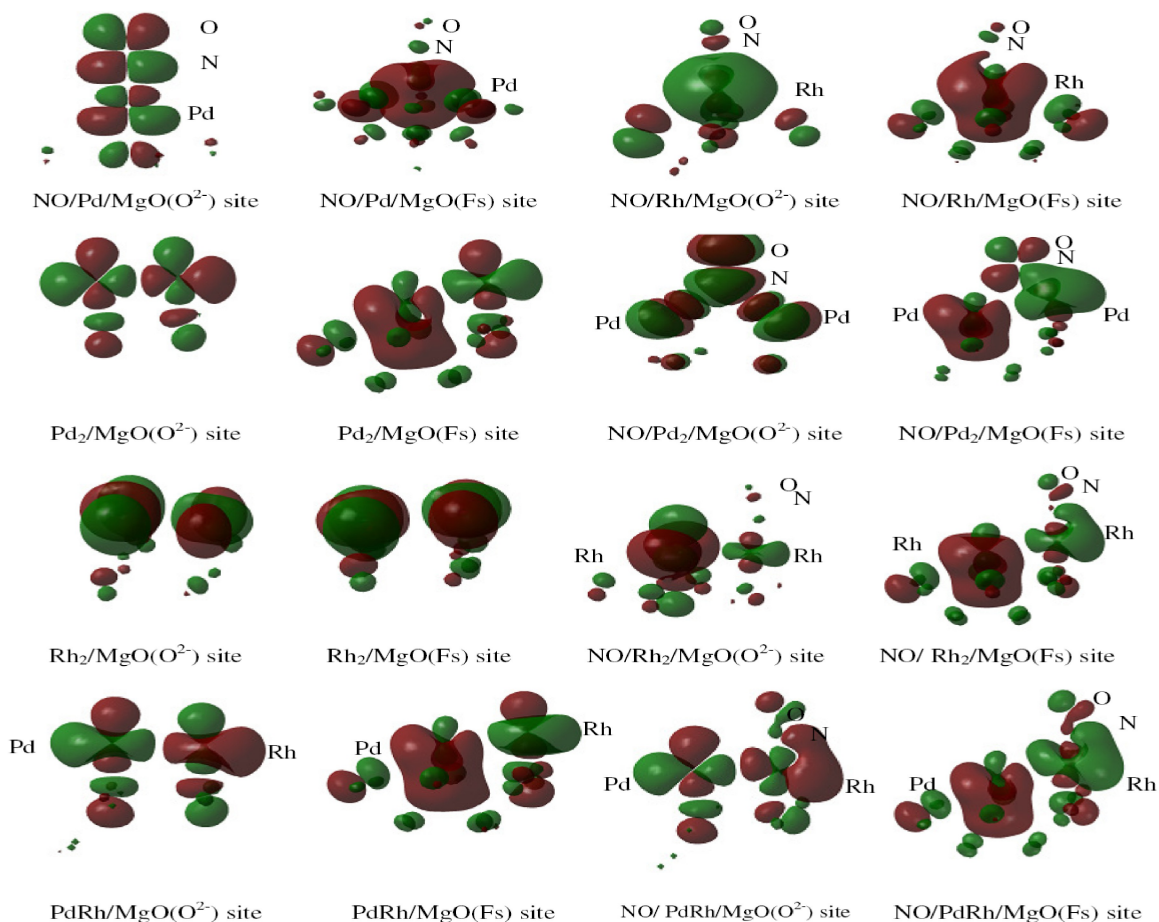


**Figure 3 :** Schematic representation of the HOMO's of Pd<sub>2</sub>/MgO, Rh<sub>2</sub>/MgO, PdRh/MgO, NO/Pd/MgO, NO/Rh/MgO, NO/Pd<sub>2</sub>/MgO, NO/Rh<sub>2</sub>/MgO and NO/PdRh/MgO deposited on MgO(O<sup>2-</sup>) and MgO(Fs) sites using the embedded cluster model.

# ORIGINAL ARTICLE

**TABLE 3 :** Transition energy,  $\Delta E_{\text{complex}}^{\text{H-L}}$ , required to excite the supported dimers, Pd<sub>2</sub>, Rh<sub>2</sub> and PdRh, from the high- to low-spin states. A positive sign indicates that the ground state is provided by the low-spin coupling.  $\Delta d_{\text{M1-s}}^{\text{H-L}}$  and  $\Delta d_{\text{M2-s}}^{\text{H-L}}$  are the change in the equilibrium distance of each TM to the surface;  $\Delta q_{\text{M1-M2}}^{\text{H-L}}$  is the change in charges at the dimers that supported to the regular (O<sup>2-</sup>) site and oxygen vacancy (Fs) site at MgO (001) going from high- to low-spin state. A positive value indicates that d and q are larger in the high-spin state. Energies are expressed in eV, the corresponding equilibrium distances (d) in (Å), and charges in electron units H: High spin. L: Low spin.

	Pd <sub>2</sub>		Rh <sub>2</sub>		PdRh	
	Pd <sub>2</sub> /MgO (O <sup>2-</sup> ) site	Pd <sub>2</sub> /MgO (Fs) site	Rh <sub>2</sub> /MgO (O <sup>2-</sup> ) site	Rh <sub>2</sub> /MgO (Fs) site	PdRh /MgO (O <sup>2-</sup> ) site	PdRh /MgO (Fs) site
( $\Delta E_{\text{complex}}^{\text{H-L}}$ ) <sup>a</sup>	2.611	3.155	-0.036	0.695	2.223	2.222
( $\Delta E_{\text{complex}}^{\text{H-L}}$ ) <sup>b</sup>	2.306	2.242	0.151	0.875	2.009	1.842
( $\Delta d_{\text{M1-s}}^{\text{H-L}}$ ) <sup>a</sup>	0.22	0.16	0.24	0.2	0.06	0.14
( $\Delta d_{\text{M1-s}}^{\text{H-L}}$ ) <sup>b</sup>	0.1	0.1	0.12	0.16	0.00	0.00
( $\Delta d_{\text{M2-s}}^{\text{H-L}}$ ) <sup>a</sup>	0.18	0.22	0.06	0.04	0.13	0.1
( $\Delta d_{\text{M2-s}}^{\text{H-L}}$ ) <sup>b</sup>	0.13	0.14	0.02	0.00	0.04	0.08
( $\Delta q_{\text{M1-M2}}^{\text{H-L}}$ ) <sup>a</sup>	0.325	0.257	0.354	0.293	0.261	0.274
( $\Delta q_{\text{M1-M2}}^{\text{H-L}}$ ) <sup>b</sup>	0.13	0.19	0.156	0.046	0.137	0.162

\*a: High spin multiplicity is (5) for Pd<sub>2</sub>, Rh<sub>2</sub> and (6) for PdRh; \*b: High spin multiplicity is (3) for Pd<sub>2</sub>, Rh<sub>2</sub> and (4) for PdRh and Where low spin state is (1) for Pd<sub>2</sub>, Rh<sub>2</sub> and (2) for PdRh

**TABLE 4 :** Adsorption properties of NO interacting with regular (O<sup>2-</sup>) site and oxygen vacancy (Fs) site of the MgO (001) surface supported Pd and Rh atoms at the low and high spin state.

	NO/ Pd				NO/ Rh			
	MgO (O <sup>2-</sup> ) site		MgO (Fs) site		MgO (O <sup>2-</sup> ) site		MgO (Fs) site	
Spin multiplicity	2	4	2	4	1	3	1	3
Spin state	L	H	L	H	L	H	L	H
E <sub>a</sub> (NO)	1.499	1.038	0.702	1.261	3.048	2.115	1.449	1.026
E <sub>a</sub> (MNO)	1.516	1.327	2.655	2.563	1.771	1.582	2.134	2.455
$\Delta E_{\text{complex}}^{\text{H-L}}$	1.695		1.598		0.934		0.423	
qMNO	-0.137	-0.126	-0.816	-0.936	-0.182	-0.063	-0.819	-0.742
d(M-S)	2.13	2.21	1.60	1.56	1.98	2.18	1.76	1.80
d(N—M)	1.90	1.96	2.06	2.02	1.74	1.82	1.78	1.96
d(N-O)	1.228	1.288	1.208	1.248	1.207	1.207	1.207	1.207

q(M): atomic charges at the adatom; q(NO): molecular charge at NO molecule; d(M-S): optimal distances between adatom and surface site of MgO; d (N-O): Equilibrium N–O distances and d(N—M): optimal distances between adatom and nitrogen atom.

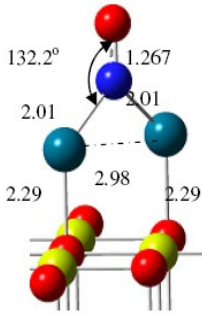
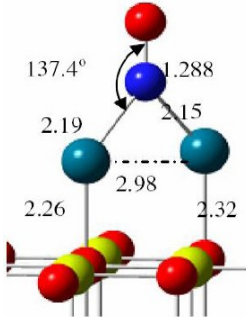
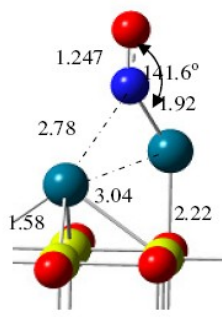
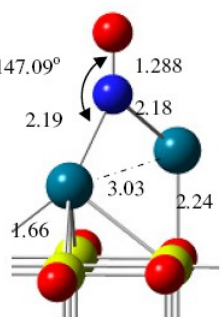
## Interaction of NO with supported Pd, Rh, Rh<sub>2</sub>, Pd<sub>2</sub> and PdRh on MgO (001)

The binding energy for the interaction of NO molecule on different spin states of Pd, Rh, Rh<sub>2</sub>, Pd<sub>2</sub> and PdRh that supported on MgO can be calculated as E<sub>a</sub>(NO) = - [E(NO/M<sub>x</sub>/MgO<sub>site</sub>) - E(M<sub>x</sub>/MgO<sub>site</sub>) - E(NO)] where x=1 or 2<sup>[55]</sup>. In all cases, the positive values correspond to exothermic processes. It is observed that NO adsorbs much more strongly at the Pd with low spin state and Rh with different spin state that deposited on the MgO (O<sup>2-</sup>) site than on the MgO (Fs),

TABLE 4. The reason of this behavior will be discussed later.

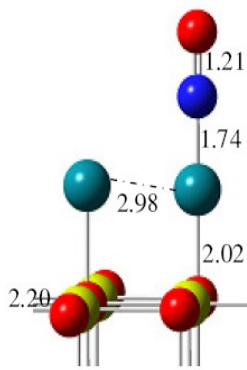
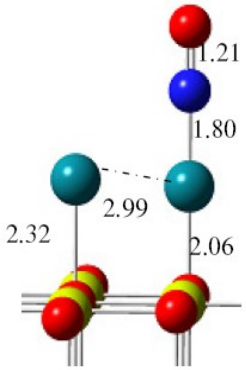
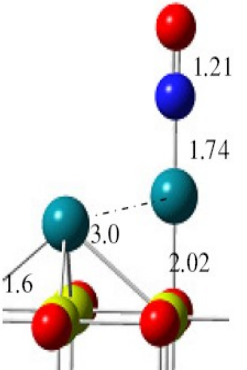
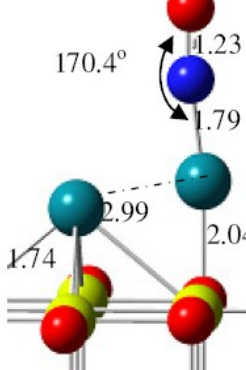
In TABLES 5-7, the adsorption energies, optimal distances and charge transfer for the interaction of NO molecule on different spin states of Rh<sub>2</sub>, Pd<sub>2</sub> and PdRh that supported at MgO (O<sup>2-</sup>) and MgO (Fs) through its N atom at various spin states have been calculated. Again, the NO molecule adsorbs much more strongly at the Pd<sub>2</sub>, with low spin state, Rh<sub>2</sub> and PdRh with different two spin state that deposited on the MgO (O<sup>2-</sup>) site than on the MgO (Fs), TABLE 5. As well as, the NO

**TABLE 5 :** Adsorption properties of NO interacting with regular ( $O^2$ ) site and oxygen vacancy (Fs) site of the MgO (001) surface supported  $Pd_2$  dimer at the low-and high spin state.

Spin multiplicity	MgO ( $O^2$ ) site		MgO (Fs) site	
	2	4	2	4
	L	H	L	H
Spin state	L	H	L	H
				
$E_a$ (NO)	1.808	1.052	1.231	1.342
$E_a$ ( $Pd_2NO$ )	1.887	2.352	3.245	3.969
Total $q(Pd_2)$	0.415	0.525	-0.493	-0.049
$q(N)$	-0.248	-0.473	-0.071	-0.460
$q(O)$	-0.27	-0.225	-0.199	-0.247
$q(NO)$	-0.518	-0.697	-0.27	-0.707
$q(Pd_2NO)$	-0.103	-0.172	-0.763	-0.756

Red spheres:  $O^2$ ; yellow spheres:  $Mg^{2+}$ ; light blue spheres: Pd atom; dark blue sphere: N atom.

**TABLE 6 :** Adsorption properties of NO interacting with regular ( $O^2$ ) site and oxygen vacancy (Fs) site of the MgO (001) surface supported  $Rh_2$  dimer at the low-and high spin state.

Spin multiplicity	MgO ( $O^2$ ) site		MgO (Fs) site	
	2	4	2	4
	L	H	L	H
Spin state	L	H	L	H
				
$E_a$ (NO)	2.909	2.506	2.971	2.097
$E_a$ ( $Rh_2NO$ )	1.786	2.542	3.607	3.885
$q(Rh_2)$	-0.164	0.01	-0.912	-0.639
$q(N)$	0.22	0.093	0.219	0.070
$q(O)$	-0.185	-0.222	-0.188	-0.231
$q(NO)$	0.035	-0.129	0.031	-0.161
$q(Rh_2NO)$	-0.129	-0.119	-0.881	-0.799

Red spheres:  $O^2$ ; yellow spheres:  $Mg^{2+}$ ; blue spheres: Rh atom; dark blue sphere: N atom.

# ORIGINAL ARTICLE

**TABLE 7 : Adsorption properties of NO interacting with regular ( $O^{2-}$ ) site and oxygen vacancy (Fs) site of the MgO (001) surface supported PdRh dimer at the low-and high spin state.**

Spin multiplicity	1	3	1	3
Spin state	L	H	L	H
	MgO ( $O^{2-}$ ) site		MgO (Fs) site	
$E_a$ (NO)	2.666	1.315	2.872	1.329
$E_a$ (PdRhNO)	2.057	2.319	3.953	3.856
$Q$ (PdRh)	-0.201	0.539	-0.901	-0.109
$Q$ (N)	0.22	-0.413	0.206	-0.359
$Q$ (O)	-0.204	-0.248	-0.205	-0.236
$Q$ (NO)	0.016	-0.661	0.001	-0.595
$Q$ (PdRhNO)	-0.184	-0.122	-0.901	-0.704

Red spheres:  $O^{2-}$ ; yellow spheres:  $Mg^{2+}$ ; light blue spheres: Pd atom; blue spheres: Rh atom; dark blue sphere: N atom.

has been adsorbed at the center of the Pd–Pd bond in a bridge position, which is energetically the most stable in agreement with previous works<sup>[37,65,73]</sup>. The Pd–Pd distance is about 2.98 Å–3.05 Å, depending on the site considered, TABLE 5. The large Pd–Pd bond distance of adsorbed  $Pd_2$  is in close agreement with the STM measurements<sup>[20]</sup>. Globally, the binding energy calculated for the adsorption of NO on the palladium dimers, 1.808 eV, is in the range of the experimental value that measured in thermal desorption by Ramsier et al.<sup>[74]</sup>.

At the high spin states a dramatic change is found when the NO which bind to the supported Pd and  $Pd_2$  where there is an increase in the binding energies at the MgO (Fs) site than on the MgO ( $O^{2-}$ ). The different behavior of Pd and  $Pd_2$  with high spin states that adsorbed on Fs centers towards NO can be explained as follows. At the low spin states of supported Pd and  $Pd_2$  the delocalization of the trapped electrons into the 5s level leads to an increased Pauli repulsion with the NO molecule and in a strong weakening of the bond. On contrary, at the supported Pd and  $Pd_2$  with high

spin states this effect is smaller because of the presence of an incomplete d shell. Figure 3 confirmed the results in TABLES 4-5 and the adsorption properties that discussed above.

Since the high occupied molecular orbital of NO is  $\pi^*$  anti-bonding orbital with an unpaired electron therefore, the charge transferred from  $Pd_2/MgO$ ,  $Rh_2/MgO$  and PdRh/MgO to the NO will occupy the  $\pi^*$  orbital and weak the NO bond strength. The NO bond length is elongated after the adsorption of NO on the particular dimers, this is consistent with the electron transfer direction<sup>[57]</sup>, TABLES 5-7. The higher electron transfer from  $Pd_2/MgO$ ,  $Rh_2/MgO$  and PdRh/MgO to NO can explain the larger stretching of the NO interatomic distance on the oxygen anion and oxygen vacancies sites.

The adsorption energy of NO on  $Rh_2/MgO$  is larger than on  $Pd_2/MgO$  (2.909 vs. 1.808 eV), possibly due the decrease of the d electrons on the Rh which can lead to a decrease of the  $\sigma$ - $\sigma$  repulsion. The metal-nitrogen bond is shorter for Rh than Pd (1.74 vs. 2.01 Å), which also indicates a strong bonding between NO and  $Rh_x/MgO$ . The larger M-N-O angle for  $Rh_2$  than

$\text{Pd}_2$  ( $180^\circ$  vs.  $132.2^\circ$ ) indicates that the  $5\sigma$  orbital is much more involved in the adsorption at Rh than Pd. These results are in agreement with<sup>[87]</sup>. Although, the charge of  $\text{Rh}_2\text{NO}$  and  $\text{Pd}_2\text{NO}$  supported on the ( $\text{O}^{2-}$ ) and (Fs) site is practically the same than that of the supported  $\text{Rh}_2$  and  $\text{Pd}_2$  at the same sites, the MgO (Fs) site acquires a much more significant negative charge, TABLES 5-7. These results are confirmed by Figure 3.

Indeed, the different behavior of rhodium and palladium supported at MgO (001) towards NO can be explained as follows. On palladium the delocalization of the trapped electrons into the  $5s$  level leads to an increased Pauli repulsion with the NO molecule and in a strong weakening of the bond, whereas on Rh this effect is smaller because of the presence of an incomplete  $d$  shell and the easier mixing of the  $5s$  with the  $4d$  orbitals to form new hybrid orbitals<sup>[62]</sup>. The high reactivity of Rh relative to Pd was also found by a periodic DFT calculation for NO adsorbed on (001) surfaces of Rh and Pd<sup>[89]</sup>. Therefore, Rh appears to be more efficient than Pd for NO adsorption at Pd–Rh bimetallic and may justify its use as a catalyst in TWC. These observations agree well with previous theoretical calculations<sup>[75]</sup>. Therefore, it seems that NO prefers binding to Rh when both Rh and Pd sites co-exist in the bimetallic Pd–Rh. These results are confirmed by TABLE 7 and Figure 3.

The optimized geometry of admolecule NO with the N-end to the Rh atom of bimetallic PdRh and the molecular axis of NO normal to the surface plane is presented in Figure 2c. The N–O distance elongates from its value of  $1.158 \text{ \AA}$  for the free NO molecule to  $1.207 \text{ \AA}$  for  $\text{Rh}_2$  and PdRh at  $\text{O}^{2-}$  and Fs, respectively. Therefore, the results show that the adsorption energies of NO at Rh–Rh and Pd–Rh, with low spin state, that deposited at  $\text{O}^{2-}$  and Fs of MgO are very close, ( $2.909$  vs.  $2.666 \text{ eV}$ ) at oxygen anion and ( $2.971$  vs.  $2.872 \text{ eV}$ ) at Fs centers, TABLES 6-7. Figure 3 confirmed the results in TABLES 2-7 with the adsorption properties discussed above.

Interestingly, the interaction is assumed to mainly be a HOMO–LUMO type<sup>[76]</sup>. The differences in the adsorption energies reported for the interaction of NO on supported PdRh at the  $\text{O}^{2-}$  and Fps center can be due to the differences in energy between the HOMO

of the surface and the LUMO of the NO molecule. The results show that, the formation of a vacancy on the MgO surface decreases the difference between the HOMO of PdRh supported at MgO (001) surface and LUMO of NO molecule by  $0.367 \text{ eV}$ . This result is in agreement with the greater strength of NO chemisorption on supported PdRh/MgO(Fs) in comparison with supported PdRh/MgO( $\text{O}^{2-}$ ), HOMO–LUMO =  $2.174 \text{ eV}$  and  $2.541 \text{ eV}$ , respectively. As the interaction of NO with PdRh occurs through a charge transfer from the HOMO of the surface to the LUMO of the adsorbed NO molecule, the smaller the value of the HOMO–LUMO gap the easier the charge transfer and consequently, the larger the adsorption energy, this is agreement with<sup>[77]</sup>.

Recently, several authors were interested in studying the CO-induced modification of the metal–MgO interaction<sup>[78,79]</sup> in the form of atoms and layers. For instance, it was reported that CO enhances the bonding between Pt or Pd atoms and the oxide, but for Au this effect is negligible<sup>[78]</sup>. To allow a similar analysis on NO, the adsorption of the  $\text{MNO}$  and  $\text{M}_2\text{NO}$  complexes on MgO (001) was considered. The corresponding binding energy can be defined in a similar way as that for  $\text{M}_x$  on MgO,  $E_a(\text{M}_x\text{NO}) = - [E(\text{NO}/\text{M}_x/\text{MgO\_site}) - E(\text{MgO\_site}) - E(\text{M}_x\text{NO})]$  where  $x=1$  or  $2$ . On terrace  $\text{O}_{5c}$  sites the  $\text{O}_{5c}\text{Rh}_2\text{NO}$  and  $\text{O}_{5c}\text{PdRhNO}$  bonds are definitely stronger than the  $\text{O}_{5c}\text{Rh}_2\text{NO}$  and  $\text{O}_{5c}\text{PdRhNO}$ . This means that an increase in temperature can lead to diffusion of the  $\text{Rh}_2\text{NO}$  and PdRhNO complexes before NO desorption occurs. Whereas on neutral F centers, the bonding of the  $\text{Pd}_2\text{NO}$ ,  $\text{Rh}_2\text{NO}$  and PdRhNO unit to the surface is so strong that no diffusion of this species occurs once the complex is trapped at an oxygen vacancy. An increase in temperature will result in the loss of NO and TM atoms filling the vacancy. An important result is that, on Fs sites, the Fs– $\text{Pd}_2\text{NO}$ , Fs– $\text{Rh}_2\text{NO}$  and Fs–PdRhNO bonding is stronger than that of the FsPd<sub>2</sub>–NO FsRh<sub>2</sub>–NO and FsPdRh–NO, TABLES 5-7.

The spin transition energies,  $\Delta E_{\text{complex}}^{\text{H-L}}$ , of ON.Pd<sub>2</sub>.MgO, ON.Rh<sub>2</sub>.MgO and ON.RhPd.MgO complexes have been considered, TABLE 8. The trend emerging from the present model calculations indicates that the metal-support interaction tends to stabilize the low-spin state with respect to the isolated atom thus,

# ORIGINAL ARTICLE

**TABLE 8 :** Transition energy,  $\Delta E_{\text{complex}}^{\text{H-L}}$ , required to excite ON.Pd<sub>2</sub>.MgO, ON.Rh<sub>2</sub>.MgO and ON.PdRh.MgO complexes from the high- to low-spin states. A positive sign indicates that the ground state is provided by the low-spin coupling.  $\Delta d_{\text{M-N}}^{\text{H-L}}$  is the change in optimal distances between TM and nitrogen atom.  $\Delta d_{\text{N-O}}^{\text{H-L}}$  is the change in optimal distances between N and O atom of NO molecule.  $\Delta q_{\text{M}_2\text{NO}}^{\text{H-L}}$  is the change in charges at the M<sub>2</sub>NO dimer that supported to the regular (O<sup>2-</sup>) site and oxygen vacancy (Fs) site at MgO (001) going from high- to low-spin state. A positive value indicates that d is larger in the high-spin state. Energies are expressed in eV, the corresponding equilibrium distances (d) in (Å), and charges in electron units H: High spin. L: Low spin.

	NO/Pd <sub>2</sub> /MgO (O <sup>2-</sup> ) site	NO/ Pd <sub>2</sub> / MgO (Fs) site	NO/Rh <sub>2</sub> /MgO (O <sup>2-</sup> ) site	NO/ Rh <sub>2</sub> / MgO (Fs) site	NO/PdRh/MgO (O <sup>2-</sup> ) site	NO/PdRh/MgO (Fs) site
( $\Delta E_{\text{complex}}^{\text{H-L}}$ (NO))	1.061	0.801	0.216	0.694	1.565	1.923
( $\Delta d_{\text{M-N}}^{\text{H-L}}$ )	0.14	0.27	0.06	0.04	0.427	0.35
( $\Delta d_{\text{N-O}}^{\text{H-L}}$ )	0.021	0.041	0	0.02	0.06	0.02
( $\Delta q_{\text{M}_2\text{NO}}^{\text{H-L}}$ )	-0.069	0.007	0.01	0.082	0.063	0.197

Where low spin multiplicity is (2) for NOPd<sub>2</sub>, NORh<sub>2</sub> and (1) for NOPdRh high spin multiplicity is (4) for NOPd<sub>2</sub>, NORh<sub>2</sub> and (3) for NOPdRh

the low-spin state becoming the ground state at regular and F<sub>s</sub> sites. Although, the combined effects of NO adsorbate and Pd<sub>2</sub>, Rh<sub>2</sub> and RhPd supported at MgO were strong enough to quench the spin of Pd<sub>2</sub>, Rh<sub>2</sub> and RhPd dimers (changes the sign of the spin transition energy), the low-spin states are preserved. Although, the interaction of ON.Rh<sub>2</sub>.MgO (Fs) and ON.RhPd.MgO (Fs) shows that the transition energy exhibits the largest increase, the interaction of ON.Pd<sub>2</sub>.MgO (Fs) exhibits the largest decrease. Notice that, as expected, there is an inverse correlation between adsorption energy and equilibrium distance, the larger the former the shorter the later, TABLES 5-8. In these cases, it is clear that the low-spin state is more favored because of the formation of a direct bond between the adsorbed transition metal dimer and the electronic levels corresponding to the oxygen vacancy electrons. The results show that the magnetic-spin states of transition metals atoms and clusters supported at metal oxide surface and the role of a precursor molecule on the considered magnetic and binding properties need to be explicitly taken into account.

## Pairwise and non-pairwise additivity

The concept of pairwise and non-pairwise additivity has been studied for atom clusters and insulators<sup>[81,82]</sup>. In studying a supported-metal catalyst system, it is very important to quantify the extent to which the support MgO (S) with regular and defective surface affects the interaction of the NO admolecule with the Pd, Rh, Pd<sub>2</sub>,

Rh<sub>2</sub> and PdRh particles. The interaction energy  $E_{(i)}^{\text{S-M}_x\text{-NO}}$  among three subsystems; the support (S), (M<sub>x</sub>) where x= 1 for Pd, Rh atom and x=2 for Pd<sub>2</sub>, Rh<sub>2</sub>, PdRh dimer, and the adsorbate (NO) molecule can be defined as:

$$E_{(i)}^{\text{S-M}_x\text{-NO}} = E^{\text{S-M}_x\text{-NO}} - E^{\text{S}} - E^{\text{M}_x} - E^{\text{NO}} \quad (5)$$

where every energy term on the right-hand side of Eq. (5) is calculated using geometrical parameters corresponding to the equilibrium geometry of S-M<sub>x</sub>-NO systems. The left-hand side represents the energy required to separate the three subsystems without altering any change in their geometrical parameters. Such energy can be divided into contributions from three-pairwise components and a non-additive term,  $\epsilon^{\text{nadd}}$ , as follows:

$$E_{(i)}^{\text{S-M}_x\text{-NO}} = E_{(i)}^{\text{S-M}_x} + E_{(i)}^{\text{S-NO}} + E_{(i)}^{\text{M}_x\text{-NO}} + \epsilon^{\text{nadd}} \quad (6)$$

where  $\epsilon^{\text{nadd}}$  is a measure of cooperative interactions among the three subsystems<sup>[38,81]</sup>. The four energy terms on the right-hand side of Eq. (6) are calculated from the relations:

$$E_{(i)}^{\text{S-M}_x} = E^{\text{S-M}_x} - E^{\text{S}} - E^{\text{M}_x} \quad (7)$$

$$E_{(i)}^{\text{S-NO}} = E^{\text{S-NO}} - E^{\text{S}} - E^{\text{NO}} \quad (8)$$

$$E_{(i)}^{\text{M}_x\text{-NO}} = E^{\text{M}_x\text{-NO}} - E^{\text{M}_x} - E^{\text{NO}} \quad (9)$$

$$\epsilon^{\text{nadd}} = E_{(i)}^{\text{S-M}_x\text{-NO}} - E_{(i)}^{\text{S-M}_x} - E_{(i)}^{\text{S-NO}} - E_{(i)}^{\text{M}_x\text{-NO}} \quad (10)$$

The total interaction energies, the pairwise energy components to the S-M<sub>x</sub>-NO systems, and the non-



**TABLE 9 :** Interaction energies of ON.Pd.MgO, ON.Rh.MgO, ON.Pd<sub>2</sub>.MgO, ON.Rh<sub>2</sub>.MgO, ON.PdRh.MgO complexes with the most stable spin states at O<sup>2-</sup> and Fs sites, pairwise components and non additivity terms. All energies are given in eV.

Complex	$E^{S-M_x-NO}$ (i)		$E^{S-M_x}$ (i)		$E^{S-NO}$ (i)		$E^{M_x-NO}$ (i)		$\epsilon^{nadd}$	
	O <sup>2-</sup>	F	O <sup>2-</sup>	F	O <sup>2-</sup>	F	O <sup>2-</sup>	F	O <sup>2-</sup>	F
ON.Pd.MgO	-2.749	-3.888	-1.238	-3.188	-0.061	-0.092	-1.229	-1.128	-0.221	0.519
ON.Rh.MgO	-4.892	-4.713	-1.294	-2.938	-0.086	-0.080	-2.570	-2.537	-0.942	0.842
ON.Pd <sub>2</sub> .MgO	-5.489	-6.847	-3.624	-5.614	0.035	-0.068	-3.529	-2.659	1.629	1.494
ON.Rh <sub>2</sub> .MgO	-5.989	-7.846	-3.058	-4.870	-0.063	-0.120	-2.528	-2.528	-0.341	-0.328
ON.PdRh.MgO	-5.704	-7.600	-3.039	-4.727	-0.062	-0.117	-2.638	-2.619	0.035	-0.136

additive energy term,  $\epsilon^{nadd}$ , are presented in TABLE 9. As shown in this table, the total interaction energies of ON.Pd.MgO<sub>13</sub>O<sup>2-</sup>, ON.Pd.MgO<sub>13</sub>Fs, ON.Rh.MgO<sub>13</sub>O<sup>2-</sup>, ON.Rh.MgO<sub>13</sub>Fs, ON.Pd<sub>2</sub>.MgO<sub>13</sub>O<sup>2-</sup>, ON.Pd<sub>2</sub>.MgO<sub>13</sub>Fs, ON.Rh<sub>2</sub>.MgO<sub>13</sub>O<sup>2-</sup>, ON.Rh<sub>2</sub>.MgO<sub>13</sub>Fs, ON.PdRh.MgO<sub>13</sub>O<sup>2-</sup> and ON.PdRh.MgO<sub>13</sub>Fs complexes are dominated by the pairwise additive components  $E_{(i)}^{S-M}$  and  $E_{(i)}^{S-M_2}$ , respectively. On

the other hand, the small values of  $E_{(i)}^{S-NO}$  pairwise component that represent the interaction energy between support (S) and admolecule (NO) in the S-M<sub>x</sub>-NO system may be attributed to the large separation between (S) and the NO admolecule. This result means that the binding of NO is mainly dominated by the  $E_{(i)}^{M_1-NO}$  and  $E_{(i)}^{M_2-NO}$  pairwise additive contributions of the considered complexes.

The non additivity term,  $\epsilon^{nadd}$ , is a measure of cooperative interaction among the subsystems, decreases with surface defect-formation at ON.Pd.MgO, ON.Rh.MgO, ON.Pd<sub>2</sub>.MgO and ON.Rh<sub>2</sub>.MgO. Except at ON.PdRh.MgO complex,  $\epsilon^{nadd}$  increases with surface defect-formation, TABLE 9. This suggests that the interaction of NO with Pd, Rh, Pd<sub>2</sub>, Rh<sub>2</sub> and PdRh dimer is essentially affected by defect formation. This confirmed the adsorption properties of NO at supported Pd, Rh, Pd<sub>2</sub>, Rh<sub>2</sub> and PdRh particles that discussed above. Finally, the role of metal oxide is not restricted only to supporting the metal, but influences the interaction of NO molecule with the Pd, Rh, Pd<sub>2</sub>, Rh<sub>2</sub> and PdRh dimers.

## CONCLUSION

An attempt has been made to understand the effect

of surface site on the spin state for the interaction of NO with Pd<sub>2</sub>, Rh<sub>2</sub> and PdRh nanoparticles that supported at regular and defective MgO (001) Surfaces. A spin-polarized treatment is considered to properly describe the ground-state electronic structure, adsorption energies and the low- to high-spin energy transition. The calculated results are compared with experimental data and previous theoretical studies as possible. The geometrical optimizations have been considered to represent the most stable structures for the adsorption of NO at the supported Pd<sub>2</sub>, Rh<sub>2</sub> and PdRh and to investigate the changes induced by the oxide substrate in the chemisorption properties of the adsorbed particles.

Upon interaction with O<sup>2-</sup> and Fs surface sites, the high to low spin transition energies of Pd atom is positive indicating that the spin states are preserved, and the low spin states are favored. Hence, the number of unpaired electrons in the adatom tends to be the same as in the gas phase and the ground state of Pd-MgO is spin singlet. However, the main contributions to the Rh atom, Pd<sub>2</sub>, Rh<sub>2</sub> and PdRh at MgO are the polarization of the metal electrons induced by the ionic substrate and the small mixing between the s and d orbitals of the transition metal with the 2p orbitals of the surface oxygen. Consequently, the interaction of Rh atom, Pd<sub>2</sub>, Rh<sub>2</sub> and PdRh dimers at MgO (001) surface induces a quenching of the magnetic moment, which results in a doublet ground state for Rh atom and PdRh as well as a singlet ground state for Pd<sub>2</sub> and Rh<sub>2</sub> at MgO (001) surface. As a consequence, the formation of the dimer in its singlet state, Rh<sub>2</sub> and Pd<sub>2</sub>, and doublet state, Pd-Rh deposited at MgO (001), is favored with respect to the presence of two isolated atoms on the surface. Notice that, as expected, there is an inverse correlation between adsorption energy and equilibrium dis-



# ORIGINAL ARTICLE

tance, the larger the former the shorter the later. In any case, the extent of metal–metal bonding in supported dimer has been increased compared with the gas-phase unit. This leads to a considerable elongation of the metal–metal bond to maximize the metal–O interaction. Notice that the dimer as a unit adsorbs much more strongly on the MgO (Fs) site than on the MgO (O<sup>2-</sup>) site. Moreover, the large enhancement in the activity of supported dimers is due mainly to the electron transfer from the cavity to the supported dimers. Theoretical calculations indicate that the formation of Rh<sub>2</sub>, Pd<sub>2</sub> and PdRh dimer on an Fs center is favored by 0.466, 0.962, and 0.807 eV respectively with respect to a TM atom bound at the Fs center and other TM atom on a terrace site. The dimers deposited interact relatively strongly with the substrate oxide forming predominantly covalent bonds with the adsorbed sites. The interaction is not accompanied by a significant charge transfer at the interface. The PdRh bimetallic have larger HOMO–LUMO gap and are relatively more chemically stable than the Pd<sub>2</sub> and Rh<sub>2</sub> monometallic that deposited on the MgO (O<sup>2-</sup>). The transition energy,  $\Delta E_{\text{complex}}^{\text{H-L}}$ , for the interaction of Pd–Rh with the oxygen anion and F<sub>s</sub> center exhibits the largest increase, 2.223 eV and 2.222 eV respectively. In these cases, it is clear that the low-spin state is more favored because of the formation of a direct bond between the adsorbed bimetallic and the electronic levels corresponding to the oxygen anion and oxygen vacancy electrons. A molecular-scale understanding of the energetic and mechanisms for formation of such metal dimers on inert oxide surfaces can open new avenues to the design of catalysts with specific functions.

In summary, it seems that NO prefers to bound with Rh atoms when both Rh and Pd site co-exist in the Pd–Rh bimetallic. The electronic structures and N–O bond lengths of the chemisorbed systems are similar for NO.Rh<sub>2</sub>.MgO and NO.PdRh.MgO with the top geometries but show significant differences from bridge geometries, NO/Pd<sub>2</sub>/MgO. Bridge-site adsorption causes the N–O bond to lengthen and soften due essentially to increase an electrostatic repulsion between both N and O atoms. In addition, the NO adsorbs much more strongly at the PdRh that is deposited on the MgO(Fs) than on the MgO(O<sup>2-</sup>) site.

The transfer of electron charge density from such a

defect to a dimer reinforces the metal–metal bonds. Therefore, color centers at the MgO surface not only reduce the diffusion of metal atoms and dimers, but also act as stabilizing agents for the whole structure. This point could be particularly important in the context of identifying methods to stabilize the support particles on an oxide substrate under chemical reaction conditions. To summarize, the larger interaction of NO at bimetallic PdRh at oxygen anions and oxygen vacancies induces an enhancement of the energy required to switch from high spin to low spin 1.565 eV and 1.923 eV respectively. These results show that the spin state of adsorbed PdRh dimer on oxide supports tends to preserve the number of unpaired electrons as found in the case of the regular terrace sites.

## ACKNOWLEDGEMENTS

The author is grateful to Deanship of Scientific Research, Qassim University to support this work. My gratitude and deep thanks to Prof. Dr. A.S. Shalabi for his interest, and useful discussions.

## REFERENCES

- [1] L.Piccolo, C.R.Henry; *Appl.Surf.Sci.*, **670**, 162 (2000).
- [2] C.Xu, W.S.Oh, G.Liu, D.Y.Kim, D.W.Goodman; *J.Vac.Sci.Technol.A*, **15**, 1261 (1997).
- [3] E.Florez, F.Mondragón, T.N.Truong, P.Fuentealba; *Surf.Sci.*, **601**, 656 (2007).
- [4] Y.Wang, E.Florez, F.Mondragón, T.N.Truong; *Surf.Sci.*, **600**, 1703 (2006).
- [5] L.Giordano, C.Di.Valentin, G.Pacchioni, J.Goniakowski; *J.Chem.Phys.*, **309**, 41 (2005).
- [6] C.Inntam, L.A.Moskaleva, K.M.Neyman, V.A.Nasluzov; *Appl.Phys.A*, **82**, 181 (2006).
- [7] H.Brune; *Surf.Sci.Rep.*, **31**, 125 (1998).
- [8] F.Cinquini, C.Di.Valentin, E.Finazzi, L.Giordano, G.Pacchioni; *Theor.Chem.Acc.*, **117**, 827 (2007).
- [9] S.Fernandez, A.Markovits, C.Minot; *Chem.Phys.Lett.*, **463**, 106 (2008).
- [10] A.Markovits, J.C.Paniagua, N.Lopez, C.Minot, F.Illas; *Phys.Rev.B*, **67**, 115417 (2003).
- [11] K.M.Neyman, C.Innatam, V.A.Nasluzov, R.Kosarev, N.Rosch; *Appl.Phys.A*, **78**, 823 (2004).
- [12] A.Markovits, M.K.Skalli, C.Minot, G.Pacchioni, N.Lopez, F.Illas; *J.Chem.Phys.*, **115**, 8172 (2001).

- [13] C.Sousa, C.de Graaf, N.Lopez, N.M.Harrison, F.Illas; *J.Phys.: Condens.Matter.*, **16**, S2557 (2004).
- [14] U.A.Paulus, U.Endruschat, G.J.Feldmeyer, T.J.Schmidt, H.Bonnemann, R.J.Behm; *J.Catal.*, **195**, 383 (2000).
- [15] S.Jalili, A.Z.Isfahani, R.Habibpour; *Computational and Theoretical Chemistry*, **989**, 18 (2012).
- [16] S.Sicolo, G.Pacchioni; *Surf.Sci.*, **602**, 2801 (2008).
- [17] Á.Kukovecz, G.Pótári, A.Oszkó, Z.Kónya, A.Erdöhelyi, J.Kiss; *Surf.Sci.*, **605**, 1048 (2011).
- [18] M.Rassoul, F.Gaillard, E.Garbowski, M.Primet; *J.Catalysis*, **203**, 232 (2001).
- [19] A.M.Ferrari; *Phys.Chem.Chem.Phys.*, **1**, 4655 (1999).
- [20] V.G.Shinkarenko, V.F.Anufrienko, G.K.Boreskov, K.G.Ione, T.M.Yureva; *Dokl.Akad.Nauk SSSR*, **223**, 410 (1975).
- [21] K.M.Neyman, F.Illas; *Catal.Today*, **105**, 2 (2005).
- [22] V.A.Nasluzov, V.V.Rivanenkov, A.B.Gordienko, K.M.Neyman, U.Birkenheuer, N.Rösch; *J.Chem. Phys.*, **115**, 8157 (2001).
- [23] A.V.Matveev, K.M.Neyman, I.V.Yudanov, N.Rösch; *Surf.Sci.*, **426**, 123 (1999).
- [24] G.Berthier; *International Journal of Quantum Chemistry*, **82(1)**, 26 (2001).
- [25] J.R.Lombardi, B.Davis; *Chem.Rev.*, **102**, 2431 (2002).
- [26] Z.J.Wu; *Chemical Physics Letters*, **406**, 24 (2005).
- [27] Z.J.Wu; *Chem.Phys.Lett.*, **383**, 251 (2004).
- [28] F.R.Negreiros, G.Barcaro, Z.Kuntová, G.Rossi, R.Ferrando, A.Fortunelli; *Surf.Sci.*, **605**, 483 (2011).
- [29] M.Y.Wang, X.J.Liu, J.Meng, Z.J.Wu; *Journal of Molecular Structure: THEOCHEM*, **804**, 47 (2007).
- [30] T.Go´mez, E.Florez, J.A.Rodriguez, F.Illas; *J.Phys. Chem.C*, **114**, 1622 (2010).
- [31] D.Die, X.Y.Kuang, J.J.Guo, B.X.Zheng; *J.Mol. Struct.(Theochem.)*, **902**, 54 (2009).
- [32] Y.H.Chin, D.L.King, H.S.Roh, Y.Wang, S.M.Heald; *J.Catal.*, **244**, 53 (2006).
- [33] F.L.Liu, Y.F.Zhao, X.Y.Li, F.Y.Hao; *J.Mol. Struct.(Theochem.)*, **809**, 189 (2007).
- [34] S.M.Vesecky, D.R.Rainer, D.W.Goodman; *J.Vac. Sci.Technol.A*, **14**, 1457 (1996).
- [35] D.R.Rainer, S.M.Vesecky, M.Koranne, W.S.Oh, D.W.Goodman; *J.Catal.*, **167**, 241 (1997).
- [36] F.Viñes, A.Desikusumastuti, T.Staudt, A.Gorling, J.Libuda, K.N.Neyman; *J.Phys.Chem.C*, **112**, 16539 (2008).
- [37] R.Grybos, L.Benco, T.Bučko, J.Hafner; *J.Comput. Chem.*, **30**, 1910 (2009).
- [38] S.Abbet, E.Riedo, H.Brune, U.Heiz, A.-M.Ferrari, L.Giordano, G.Pacchioni; *J.Am.Chem.Soc.*, **123**, 6172 (2001).
- [39] T.Mineva, V.Alexiev, C.Lacaze-Dufaure, E.Sicilia, C.Mijoule, N.Russo; *J.Molecular Structure: THEOCHEM*, **903**, 59 (2009).
- [40] N.Lopez, F.Illas; *J.Chem.Phys.B*, **102**, 1430 (1998).
- [41] A.D’Ercole, E.Giamello, C.Pisani, L.Ojamae; *J.Phys.Chem.*, **103**, 3872 (1999).
- [42] W.S.Abdel Halim, S.Abdel Aal, A.S.Shalabi; *Thin Solid Films*, **516**, 4360 (2008).
- [43] A.D.Becke; *J.Chem.Phys.*, **98**, 5648 (1993).
- [44] C.Lee, W.Yang, R.G.Parr; *Phys.Rev.B*, **37**, 785 (1988).
- [45] N.Lopez, F.Illas, N.Rösch, G.Pacchioni; *J.Chem. Phys.*, **110**, 4873 (1999).
- [46] I.P.R.Moreira, F.Illas, R.L.Martin; *Phys.Rev.B*, **65**, 1551021 (2002).
- [47] P.E.Siegbahn, R.H.Crabtree; *J.Am.Chem.Soc.*, **119**, 3103 (1997).
- [48] F.Illas, I.P.R.Moreira, C.Graaf, V.Barone; *Theor. Chem.Acc*, **104**, 265 (2000).
- [49] W.Stevens, M.Krauss, H.Basch, P.G.Jasien; *Can.J. Chem.*, **70**, 612 (1992).
- [50] T.R.Cundari, W.J.Stevens; *J.Chem.Phys.*, **98**, 5555 (1993).
- [51] G.Larsen; *Can.J.Chem.*, **78**, 206 (2000).
- [52] V.E.Henrich, P.A.Cox; *The Surface Science of Metal Oxides*, Cambridge University Press, Cambridge, (1994).
- [53] R.W.Grimes, C.R.A.Catlow, A.M.Stoneham; *J.Chem.Soc., Faraday Trans. II*, **85**, 485 (1989).
- [54] M.J.Frisch et. al.; *Gaussian 09*, Gaussian Inc, Pittsburgh, PA, (2009).
- [55] S.A.Fuente, R.M.Ferullo, N.F.Domancich, N.J.Castellani; *Surf.Sci.*, **605**, 81 (2011).
- [56] L.Giordano, G.Pacchioni; *Surf.Sci.*, **575**, 197 (2005).
- [57] A.Silvia, G.Patricia, M.Ferullo, J.Castellani; *Surf.Sci.*, **602**, 1669 (2008).
- [58] M.Yulikov, M.Sterr, M.Heyde, H.-P.Rust, T.Risse, H.-J.Freund, G.Pacchioni, A.Scagnelli; *Phys.Rev. Lett.*, **96**, 146804 (2006).
- [59] M.Moseler et al.; *Phys.Rev.Lett.*, **89**, 176103 (2002).

**ORIGINAL ARTICLE**

- [60] L.Xua, G.Henkelman, C.T.Campbell, H.Jónsson; *Surf.Sci.*, **600**, 1351 (2006).
- [61] A.Stirling, I.Gunji, A.Endow, Y.Oumi, M.Kubo, A.Miyamoto; *J.Chem.Soc.Faraday Trans.*, **93**, 1175 (1995).
- [62] L.Giordano, A.D.Vitto, G.Pacchioni, A.M.Ferrari; *Surf.Sci.*, **540**, 63 (2003).
- [63] A.Reed, R.B.Weinstock, F.Weindhold; *J.Chem. Phys.*, **83**, 735 (1985).
- [64] S.Zhao, Y.Ren, Y.Ren, J.Wang, W.Yin; *Comp. Theor.Chem.*, **964**, 298 (2011).
- [65] C.Dufaurea, J.Roques, C.Mijoule, E.Sicilia, N.Russo, V.Alexiev, T.Mineva; *J.Mole.Catal.A: Chemical*, **341**, 28 (2011).
- [66] L.Giordano, C.Di.Valentin, J.Goniakowski, G.Pacchioni; *Phys.Rev.Lett.*, **92**, 096105 (2004).
- [67] W.Zhang, Q.Ge, L.Wang; *J.Chem.Phys.*, **118**, 5793 (2003).
- [68] V.Kumar, Y.Kawazoe; *Phys.Rev.B*, **66**, 144413 (2002).
- [69] J.X.Yang, F.W.Cheng, J.J.Guo; *Physica B*, **405**, 4892 (2010).
- [70] A.Bogicevic, D.R.Jennison; *Surf.Sci.*, **515**, L481 (2002).
- [71] I.Efremenko; *J.Mol.Catal.A Chem.*, **173**, 19 (2001).
- [72] L.Piccolo, C.R.Henry; *J.Mol.Catal.A Chem.*, **167**, 181 (2001).
- [73] C.Dufaurea, J.Roques, C.Mijoule, E.Sicilia, N.Russo, V.Alexiev, T.Mineva; *J.Mole.Catal.A: Chemical*, **341**, 28 (2011).
- [74] R.D.Ramsier, H.N.Q.Gao, K.W.Lee, O.W.Nooji, L.Lefferts, J.T.Yates; *Surf.Sci.*, **320**, 209 (1994).
- [75] M.H.Tsai, K.C.Hass; *Phys.Rev.B*, **51**, 14616 (1995).
- [76] G.Pacchioni; *Surf.Sci.*, **281**, 207 (1993).
- [77] E.Florez, P.Fuentealba, F.Mondragón; *Catal.Today*, **133**, 216 (2008).
- [78] M.Sterrer, M.Yulikov, T.Risse, H.J.Freund, J.Carrasco, F.Illas, C.D.Valentin, L.Giordano, G.Pacchioni, T.Risse, H.J.Freund; *Angew.Chem. Int.Ed.*, **45**, 2633 (2006).
- [79] H.Grönbeck, P.Broqvist; *J.Phys.Chem.B*, **107**, 12239 (2003).
- [80] S.Abbeta, U.Heizb, A.M.Ferrari, L.Giordanod, C.Di.Valentin, G.Pacchioni; *Thin Solid Films*, **400**, 37 (2001).
- [81] W.S.Abdel Halim, M.M.Assem, A.S.Shalabi, K.A.Soliman; *Appl.Surf.Sci.*, **255**(17), 7547 (2009).
- [82] A.S.Shalabi, E.M.Nour, W.S.Abdel Halim; *Int.J. Quantum Chemistry*, **76**(1), 10 (2000).